2015

Strategies for Increasing the Néel Temperature of Magnetoelectric Fe_2TeO_6

Sai Mu
University of Nebraska-Lincoln

Kirill D. Belashchenko
University of Nebraska-Lincoln, belashchenko@unl.edu

Published in *Journal of Physics: Condensed Matter* 27, 022203 (2015), 5 pp.; doi: 10.1088/0953-8984/27/2/022203

Submitted October 24, 2014; revised November 20, 2014; accepted November 25, 2014; published December 15, 2014.

Strategies for Increasing the Néel Temperature of Magnetoelectric Fe_2TeO_6

Sai Mu and Kirill D. Belashchenko

Department of Physics and Astronomy and Nebraska Center for Materials and Nanoscience, University of Nebraska–Lincoln, Lincoln, Nebraska, USA

Corresponding author – Kirill D. Belashchenko, email belashchenko@unl.edu

Abstract

Ways to increase the Néel temperature T_N in the magnetoelectric Fe_2TeO_6 antiferromagnet are explored with the help of first-principles calculations. Substitution of larger ions like Zr or Hf for tellurium increases the superexchange angles. The compensating O vacancies tend to form bound complexes with Zr dopants, which do not degrade the electronic band gap. T_N is estimated to increase by 15% at 12.5% Te → Zr substitution with such compensation. Substitution of N for O is favorable due to the decreased charge-transfer gap. The overall effect for N^{3-} substitution compensated by O vacancies is estimated at 3–4% T_N enhancement per 1% O → N substitution. A 1% compressive (0 0 1) epitaxial strain enhances T_N by about 6%.

Keywords: magnetoelectric antiferromagnet, first-principles calculations, superexchange

Spintronic device applications usually employ ferromagnets as active magnetic elements [1], but alternative schemes based on antiferromagnetic materials are also possible [2–7]. Antiferromagnets are used to provide an exchange bias [8] for pinned ferromagnetic layers in spin valves and tunnel junctions. Of particular interest are magnetoelectric [9, 10] antiferromagnets enabling voltage-controlled switching of exchange bias [11] with potential applications in nonvolatile memory [12, 13] and other devices.

The lack of magnetoelectric antiferromagnets suitable for room-temperature operation motivated the search for alloying elements to increase the Néel temperature T_N of the

"first-choice" magnetoelectric Cr_2O_3 beyond its normal value of 307 K. A strong favorable effect of boron doping predicted theoretically for this material [14] was recently corroborated experimentally [15].

In this article we turn to Fe_2TeO_6, a magnetoelectric antiferromagnet with the trirutile lattice and T_N of about 210 K [16]. The demonstration of electric-field control of spin polarization in the x-ray magnetic circular dichroic signal from Fe_2TeO_6 surface [17] showed that this material is potentially suitable for switchable exchange bias applications. Our present goal is to develop strategies for increasing the Néel temperature of Fe_2TeO_6.

First-principles calculations were carried out using the projector augmented-wave (PAW) method [18] implemented in the Vienna *ab initio* simulation package (VASP) [19, 20]. The 3*d* states of Fe were treated within the LDA + U method [21].

First we address the magnetic properties of ideal Fe_2TeO_6. Its body-centered tetragonal crystal lattice can be represented as a $Fe_\uparrow Fe_\downarrow Te$ [0 0 1] cation superlattice within the parent rutile lattice (Figure 1(*a*)). Each Fe atom has one nearest Fe neighbor and four next-nearest Fe neighbors connected by superexchange paths shown in Figure 1(*b*). Calculations with the constrained occupations of the Fe 3*d* states treated in the atomic limit give the values $U = 6.0$ eV and $J = 0.9$ eV. The full and partial densities of states (DOS) calculated with these parameters are plotted in Figure 2. The top of the valence band is dominated by O 2*p* states, while empty Fe 3*d* states form the bottom of conduction band. The charge-transfer band gap is about 1.7 eV. The 3*d* states of Fe are half-filled, resulting in a high-spin state with the 4.3 μ_B local spin moment in good agreement with the experimental value of 4.2 μ_B [22]. The large deviation from the 5μB ionic limit is due to the hybridization of the Fe 3*d* and O 2*p* states, which is evident in the partial DOS.

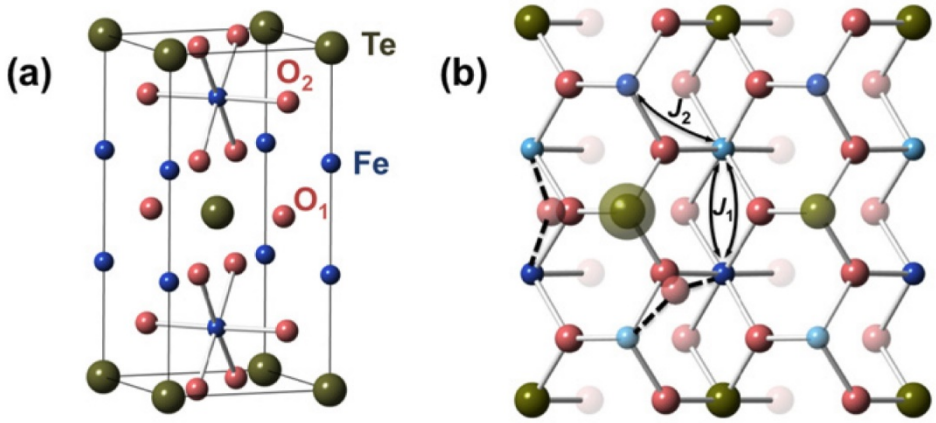

Figure 1. (*a*) Tetragonal unit cell of Fe_2TeO_6. (*b*) Side view of the 2 × 2 × 1 supercell. Arrows: superexchange paths for J_1 and J_2. Dashed lines: lattice distortion near a large impurity like Zr on the Te site (sketch).

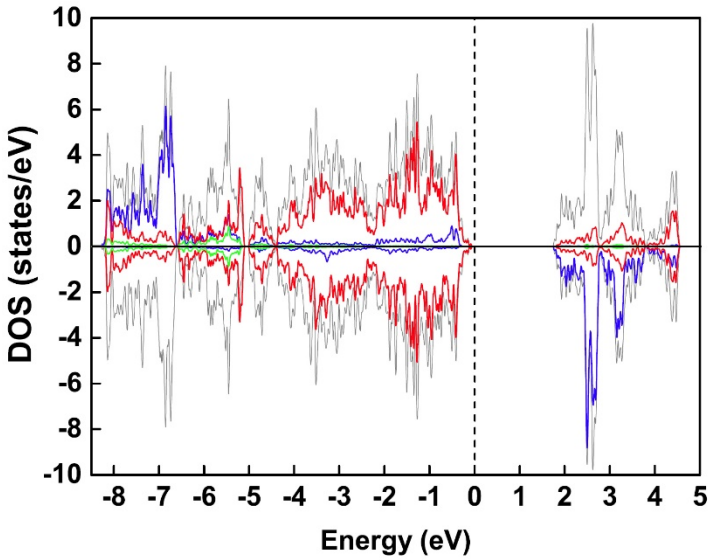

Figure 2. Density of states (DOS) in Fe_2TeO_6. Gray line: total DOS per formula unit. Blue, red, and green lines show partial DOS for Fe, O (times 6), and Te, respectively.

To evaluate the exchange interaction parameters and to study the effects of chemical substitution, we set up a 72-atom 2 × 2 × 1 supercell whose side view is shown in Figure 1(*b*). The Heisenberg exchange parameters J_n are fitted to the calculated total energies of 14 collinear spin configurations in this supercell. (The J_n are normalized so that an n-shell pair of parallel spins contributes $(5/2)^2 J_n$ to the total energy.) The Néel temperature is estimated using the spin-5/2 pair cluster approximation [23], which takes into account the pairwise spin correlations in the spirit of the Bethe-Peierls approximation; see [24] for its application to Cr_2O_3.

The key properties are listed in Table 1 for several values of U. The volume and the bond angles (not listed) are insensitive to U; the volume is underestimated by about 3% compared to experiment [25].

Table 1. Exchange parameters J_n (meV) as a function of U (eV) at $J = 0.9$ eV. CV: take-one-out cross-validation score (meV) for each fit. The atomic volume Ω (Å^3/atom), the Fe spin moment μ_{Fe} (μ_B), the band gap ε_g (eV), and the calculated Néel temperature T_N (K) are also listed.

U	Ω	μ_{Fe}	ε_g	J_1	J_2	J_3	J_4	J_5	CV	T_N
4.0	10.42	4.11	1.42	3.41	4.66	0.81	0.72	0.31	0.3	379
5.0	10.41	4.21	1.56	2.82	3.82	0.63	0.52	0.21	0.3	329
6.0	10.38	4.30	1.69	2.19	3.16	0.51	0.42	0.15	0.2	281
7.0	10.34	4.39	1.87	1.68	2.58	0.41	0.34	0.11	0.5	234
8.0	10.27	4.50	2.03	1.29	2.09	0.32	0.26	0.08	0.1	191

The dominant exchange couplings J_1 and J_2 correspond to Fe atoms directly linked by O. At $U = 6$ eV we find $T_N = 281$ K, which exceeds the experimental value [16] by 34%. T_N

decreases quickly with increasing U due to the suppression of the p-d hybridization, which also increases the Fe spin moment. The calculated value $U = 6$ eV was used in further computations.

We now turn to the possible strategies for increasing T_N in Fe_2TeO_6, which is the main focus of this article. Since superexchange is maximized for half-filled 3d shells, substitution of other elements for Fe would be counterproductive. On the other hand, superexchange originates in the electronic processes that are fourth-order in the p-d overlap integrals t_{pd} with energy denominators containing powers of the p-d charge-transfer gap Δ [26]. Therefore, superexchange can be strengthened by increasing t_{pd} or by decreasing Δ. In the following we explore both of these options through suitable Te and O substitutions.

To assess the effect of an impurity on T_N, we use the approach of [14] and calculate the exchange energies for different Fe atoms in the supercell, defined as the energy cost of reversing the spin moment on a particular atom. It is then assumed that T_N is proportional to the exchange energy averaged over all Fe atoms. The atomic positions are fixed at their optimized values for the antiferromagnetic state with the given impurities.

Each Fe atom has one nearest Fe neighbor and four next-nearest neighbors (Figure 1(*b*)). The J_1 interaction is mediated by two O_1 atoms in the TeO_2 layer, and J_2 by one O_2 atom. The bond angles are 98° and 128° for Fe–O_1–Fe and Fe–O_2–Fe exchange paths, respectively. According to the Goodenough-Kanamori rules [27], a 180° bond angle is optimal for antiferromagnetic superexchange due to the maximization of the σ-bonding overlap integrals t_{pd}. This is consistent with J_2 being dominant. While for the 90° bond angle the σ-bonding superexchange is suppressed, there are several weaker superexchange mechanisms of different sign for two d^5 ions [27]. The fact that J_1 is still strongly antiferromagnetic in spite of the bond angle being close to 90° suggests that the antiferromagnetic contribution from direct 3d-3d hopping also contributes to J_1.

Since the Fe–O–Fe bond angles are far from optimal, our first strategy is to increase them by a suitable substitution. As indicated in Figure 1(*b*), this can be achieved by substituting a larger ion for Te, which would push its O neighbors outward and thereby straighten the Fe–O–Fe bonds. Unfortunately, isoelectronic larger-ion substitutions for Te are unavailable; Mo and W are isoelectronic, but we found they have little effect on the Fe–O–Fe angles and T_N. We therefore consider group-IV (Zr, Hf) and group-V (Nb, Ta) substitutions. These defects should be compensated to preserve electric insulation.

The substitution is implemented by replacing one of the eight Te atoms in the 72-atom supercell by the dopant (Figure 1(*b*)). Let us focus on Zr (Hf is similar). The uncompensated Zr impurity introduces two holes: a mid-gap impurity level and a shallow donor level which blends with the valence band in our supercell, turning it metallic. Such shallow donor states are undesirable for applications because they easily degrade the electric insulation. We therefore consider a Zr^{4+} defect state by adding a positive charge $2e$ as homogeneous background representing the presence of yet unspecified compensating defects. The extra charge fills the hole states introduced by Zr. As a result of the ensuing structural relaxation, the mid-gap state moves down and blends with the valence band. A full insulating band gap with no impurity levels is thereby restored. This favorable property is shared by Hf^{4+}, Nb^{5+}, and Ta^{5+} impurities.

Table 2 shows that the Fe–O bond lengths decrease and the Fe–O–Fe angles increase near the Zr^{4+} impurity, leading to a 24% increase in T_N. The Hf^{4+} impurity has a similar but slightly smaller effect. Group-V impurities (Nb and Ta) are about twice less efficient, while group-VI Mo and W have nearly no effect on T_N.

Table 2. Fe–O bond lengths (Å) and Fe–O–Fe bond angles near the impurity in the $Fe_{16}XTe_7O_{48}$ supercell. The last column (η) shows the estimated increase of T_N.

X	Fe–O_1	Fe–O_2	Fe–O_1–Fe	Fe–O_2–Fe	η, %
Te	1.97	1.97, 1.99	98.3°	128.3°	0
Mo	1.96	1.97, 2.00	97.9°	126.9°	3.6
Nb^{5+}	1.92	1.92, 1.96	100.2°	130.6°	10.7
Zr^{4+}	1.88	1.91, 1.91	103.7°	136.3°	23.8
W	1.96	1.96, 1.99	97.9°	127.2°	–3.3
Ta^{5+}	1.92	1.92, 1.96	100.2°	130.8°	10.2
Hf^{4+}	1.88	1.88, 1.91	102.7°	134.8°	21.4

Oxygen vacancies (VO) can serve as compensating defects for group-IV and group-V impurities. In particular, an O vacancy can donate two electrons to compensate the two holes introduced by a Zr impurity. Figure 3 shows the total energy of the 72-atom supercell with one Zr (or Hf) impurity and one O vacancy as a function of the distance between the two defects. The lowest energy corresponds to the O vacancy located at the O_2 site next to Zr. Transferring the vacancy to the O_1 site next to Zr costs almost 0.4 eV, and moving it farther away at least 0.7 eV. Clearly, O vacancies tend to associate in strongly bound complexes with oppositely charged Zr impurities.

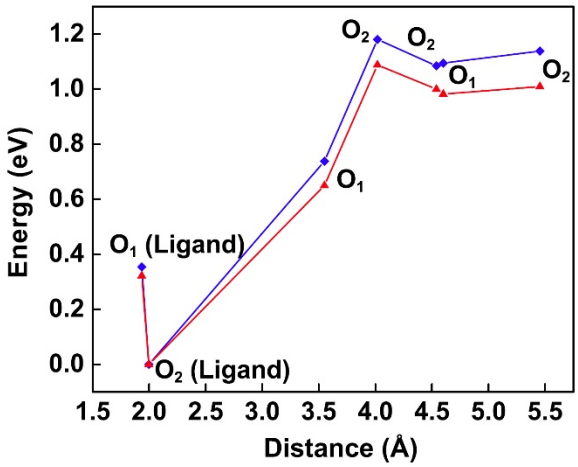

Figure 3. Total energy of a supercell with one Zr (or Hf) impurity and one O vacancy as a function of the distance between the two defects. Blue line: Zr; red: Hf. The ground state energy is taken as zero.

The free energy of vacancy formation can be controlled by the partial pressure of oxygen gas. It is seen from Figure 3 that there is a wide range of oxygen chemical potential such that the formation of a vacancy in the O_2 site near Zr lowers the free energy, while unbound O vacancies are unfavorable. Annealing at the corresponding oxygen pressure can therefore be used to promote the binding of one O vacancy to each Zr impurity while keeping the unbound vacancy concentration low. The DOS of a supercell with one stable Zr–VO_2 complex (not shown) has no impurity levels in the band gap. The same applies to the nearest-neighbor Zr–VO_1 complex with the next-lowest energy. Therefore, such complexes are not detrimental to the electric insulation of the material.

An undesirable side effect of the O vacancies is the deletion of the superexchange paths mediated by the missing oxygen atoms. The net effect on the T_N is, however, still positive: the replacement of one Te by a stable Zr–VO_2 complex in the 72-atom supercell leads to a 15% enhancement of T_N. Similar conclusions apply to Hf impurities.

Another way to increase T_N is to add anion impurities with a smaller 2*p* binding energy and hence a smaller *p*-*d* charge-transfer energy. In order to preserve the antiferromagnetic superexchange, the anion 2*p* states should remain filled. Thus, the anion 2*p* states should be raised but not too much, which suggests nitrogen substitution.

Calculations for the 72-atom supercell show that the substitution of N at the O_2 site has a lower energy compared to the O_1 site by 132 meV and is therefore more favorable. The following results are presented for this case, but in all important aspects they are similar for O_1 substitution. The DOS for N substitution at O_2 is shown in Figure 4 for two charge states: N^{2-} (neutral supercell) and N^{3-} (extra charge e added as positive background). A N^{2-} dopant introduces an empty mid-gap impurity level, which is strongly localized on the N atom. There is also an occupied level close to the valence band maximum. The N atom has a large local spin moment of 0.5 μ_B due to the localized spin-polarized hole.

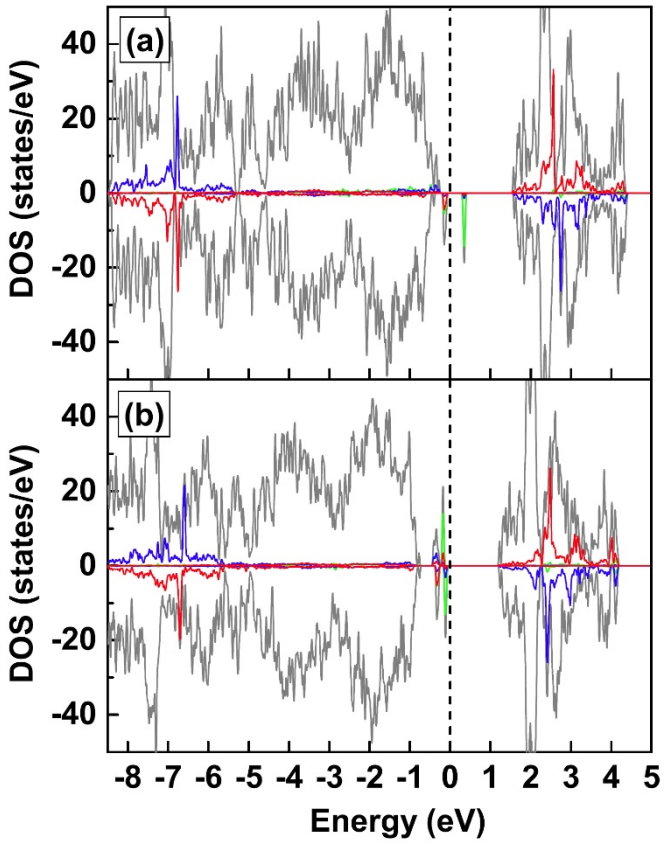

Figure 4. DOS for the N dopant at the O_2 site in Fe_2TeO_6: neutral state (upper panel) and the state with one extra electron (lower panel). Gray line: total DOS; green line: partial DOS for N; blue and red lines: partial DOS for the two Fe neighbors of N. All partial DOS are scaled by factor 2.

The addition of one electron (N^{3-} charge state) splits off two more localized states from the valence band. As seen from Figure 4, the excitation gap is significantly larger in this charge state, which should lead to better electric insulation, although it is still reduced by about 50% compared to the bulk band gap. The raising and complete filling of the N 2*p* states can both be expected to strengthen the antiferromagnetic superexchange interaction; this is confirmed by the data in Table 3.

Table 3. Fe–N–Fe bond angle, Fe–N bond lengths d_i (Å), and exchange energies (E_i, meV) for the two Fe neighbors of the N dopant, compared with the undoped case.

Dopant	Bond angle	d_1	d_2	E_1	E_2
O	128.3°	1.97	1.99	164	164
N^{2-}	131.2°	1.97	2.00	212	264
N^{3-}	130.1°	1.90	1.88	310	322

The exchange energies of the two Fe neighbors of N are larger for the N^{2-} state compared to the undoped case, and larger still for the N^{3-} impurity. Although the N^{3-} impurity shortens the bonds and slightly increases the bond angle, these changes have little effect on the exchange energies. Indeed, we found the exchange energies E_1 and E_2 become only 3–4% larger compared to bulk Fe_2TeO_6 if N is replaced back by O while fixing the atomic positions. Thus, the enhanced exchange coupling is due to the reduced charge-transfer energy. Note that the exchange energies are already enhanced in the N^{2-} charge state, even though a partially filled 2*p* orbital should make a ferromagnetic contribution to exchange interaction. This is explained by the fact that the empty impurity orbital has a weaker $(p–d)\pi$ bonding character.

Using the averaged exchange energies, we estimate the T_N increases by 2–3% or 5–6% for substitution at a 1% N–O ratio in the N^{2-} or N^{3-} charge state, respectively. Clearly, the N^{3-} state is preferable, but in practice these defects need to be compensated. Since one O vacancy is required to compensate two N^{3-} dopants, we refrain from studying the possible defect complexes here. If the negative effect of O vacancies on T_N is similar to the compensated Zr case, the overall effect of vacancy-compensated N^{3-} should be reduced to 3–4% at the 1% N–O ratio.

We now consider the effect on T_N of mechanical strain $u_{\alpha\beta}$, which changes the overlap integrals t_{pd} through changes in bond lengths and geometry. Strain-induced changes in T_N are described by a second-rank tensor, which in a tetragonal crystal has two independent components: $\delta T_N = \eta_z u_{zz} + \eta\perp(u_{xx} + u_{yy})$. In order to determine η_z and $\eta_\perp$, we consider two stress modes preserving the tetragonal symmetry: epitaxial stress (vanishing σ_{zz} stress component) and uniaxial stress (vanishing σ_{xx} and σ_{yy}). All atomic positions are relaxed along with the lattice parameter in the direction of vanishing stress.

The uniaxial stress has almost no effect on T_N, so we only display the epitaxial strain results in Figure 5. As expected for this strain mode, the in-plane Fe–O_2 bonds expand or contract in proportion to the in-plane strain, while other Fe–O bond lengths are almost unchanged. Under epitaxial compression, the Fe–O_1–Fe bond angle increases due to the increase in the *c* parameter, and therefore J_1 increases. Although the Fe–O_2–Fe angle decreases at a rate of 2° per 1% compressive strain, J_2 also increases due to the contraction of the in-plane Fe–O_2 bonds. The dependence of J_1 on strain is strongly nonlinear on the tensile side, with J_1 passing through a minimum at 3% strain. This is likely due to the antiferromagnetic contribution from direct 3*d*-3*d* hopping, which is promoted by shorter nearest-neighbor Fe–Fe distance.

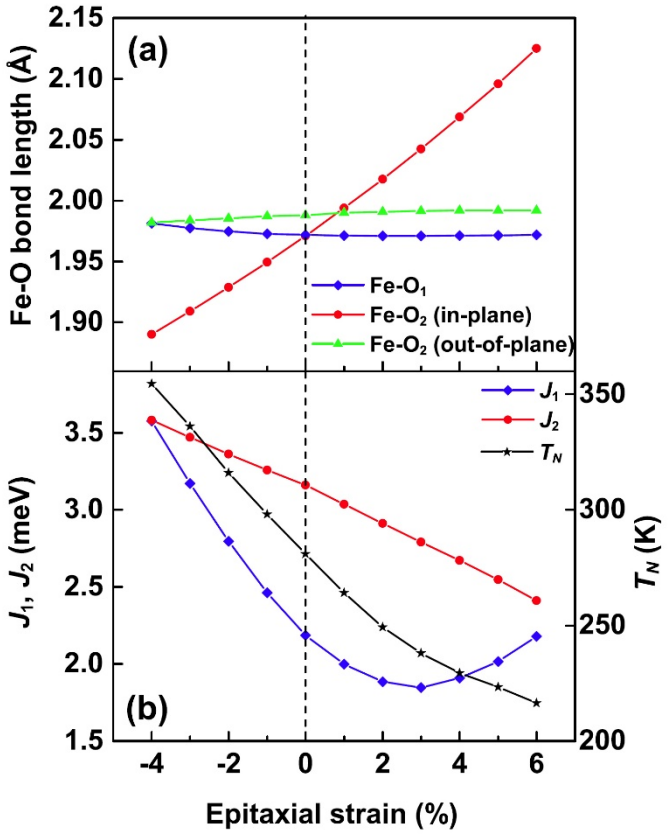

Figure 5. (*a*) Fe–O bond lengths and (*b*) J_1, J_2, and T_N as a function of epitaxial strain.

In the linear region T_N increases at a rate of 6% per 1% epitaxial compression and is almost constant under uniaxial stress. In terms of pressure, $dT_N/dp_a = dT_N/dp_b = 0.25$ K/kbar, $dT_N/dp_c < 0.01$ K/kbar. The tensor components defined above are $\eta_z = -700$K and $\eta_\perp = -1160$ K.

In conclusion, the Néel temperature of Fe_2TeO_6 can be enhanced while maintaining electric insulation by (1) substitution of larger ions like Zr for Te with full compensation by O vacancies by tuning the oxygen gas pressure, (2) substitution of N for O, perhaps also compensated by O vacancies, and (3) compressive (0 0 1) epitaxial strain.

Acknowledgments – This work was supported by the Center for NanoFerroic Devices (CNFD) and the Nanoelectronics Research Initiative (NRI) and performed utilizing the Holland Computing Center of the University of Nebraska.

References

[1] Žutić I, Fabian J and Das Sarma S 2004 *Rev. Mod. Phys.* 76 323

[2] Núñez A S, Duine R A, Haney P and MacDonald A H 2006 *Phys. Rev.* B 73 214426

[3] Shick A B, Khmelevskyi S, Mryasov O N, Wunderlich J and Jungwirth T 2010 *Phys. Rev.* B 81 212409

[4] Barthem V M T S, Colin C V, Mayaffre H, Julien M-H and Givord D 2013 *Nat. Commun.* 4 2892

[5] Wadley P et al 2013 *Nat. Commun.* 4 2322

[6] Wu H-C, Liao Z-M, Sofin R G S, Feng G, Ma X-M, Shick A B, Mryasov O N and Shvets I V 2012 *Adv. Mater.* 24 6374

[7] Park B G et al 2011 *Nat. Mater.* 10 347

[8] Nogués J et al 2005 *Phys. Rep.* 422 65

[9] Landau L D and Lifshitz E M 1960 *Electrodynamics of Continuous Media* (Oxford: Pergamon)

[10] Fiebig M 2005 *J. Phys.* D 38 R123

[11] He X et al 2010 *Nat. Mater.* 9 579

[12] Binek Ch and Doudin B 2005 *J. Phys.: Condens. Matter* 17 L39

[13] Bibes M and Barthélémy A 2008 *Nat. Mater.* 7 425

[14] Mu S, Wysocki A L and Belashchenko K D 2013 *Phys. Rev.* B 87 054435

[15] Street M et al 2014 *Appl. Phys. Lett.* 104 222402

[16] Buksphan S, Fischer E and Hornreich R 1972 *Solid State Commun.* 10 657

[17] Wang J et al 2014 *J. Phys.: Condens. Matter* 26 055012

[18] Blöchl P E 1994 *Phys. Rev.* B 50 17953

[19] Kresse G and Hafner J 1993 *Phys. Rev.* B 48 13115

[20] Kresse G and Furthmüller J 1996 *Phys. Rev.* B 54 11169

[21] Liechtenstein A I, Anisimov V I and Zaanen J 1995 *Phys. Rev.* B 52 R5467

[22] Kunnmann W, La Placa S, Corliss L M and Hastings J M 1968 *J. Phys. Chem. Solids* 29 1359

[23] Vaks V G and Zein N E 1975 *Sov. Phys.—JETP* 40 537

[24] Shi S, Wysocki A L and Belashchenko K D 2009 *Phys. Rev.* B 79 104404

[25] Krishnan K, Mudher K D S, Rao G A R and Venugopal V 2001 *J. Alloys Compounds* 316 264

[26] Maekawa S, Tohyama T, Barnes S, Ishihara S, Koshibae W and Khaliullin G 2004 *Physics of Transition Metal Oxides* (*Springer Series in Solid State Sciences*) vol 144 (Berlin: Springer)

[27] Goodenough J B 1958 *J. Phys. Chem. Solids* 6 287; Kanamori J 1959 *J. Phys. Chem. Solids* 10 87